



1 **Thermodynamics of Saline and Fresh Water Mixing in Estuaries**

2  
3 Zhilin Zhang and Hubert H.G. Savenije  
4 Delft University of Technology

5 **Abstract**

6 Mixing of saline and fresh water is a process of energy dissipation. The fresh water flow that enters  
7 an estuary from the river contains potential energy with respect to the saline ocean water. This  
8 potential energy is able to perform work. Looking from the ocean to the river, there is a gradual  
9 transition from saline to fresh water and an associated rise of the water level in accordance with the  
10 increase of potential energy. Alluvial estuaries are systems that are free to adjust dissipation  
11 processes to the energy sources that drive them, primarily the kinetic energy of the tide and the  
12 potential energy of the river flow, and to a minor extent the energy in wind and waves. Mixing is  
13 the process that dissipates the potential energy of the fresh water. The Maximum Power (MP)  
14 concept assumes that this dissipation takes place at maximum power, whereby the different mixing  
15 mechanisms of the estuary jointly perform the work. In this paper, the power is maximized with  
16 respect to the dispersion coefficient that reflects the combined mixing processes. The resulting  
17 equation is an additional differential equation that can be solved in combination with the advection-  
18 dispersion equation, requiring only two boundary conditions for the salinity and the dispersion. The  
19 new equation has been confronted with 52 salinity distributions observed in 23 estuaries in different  
20 parts of the world and performed very well, even better than the well-tested empirical Van der  
21 Burgh equation that required a calibration parameter, which with this equation is no longer needed.  
22  
23  
24  
25

26 **1. Introduction**

27 Mixing of fresh and saline water in estuaries is governed by the dispersion-advection equation,  
28 which results from the combination of the salt balance and the water balance under partial to well-  
29 mixed conditions (see e.g. Savenije, 2005). The partially to well-mixed condition applies when the  
30 increase of the salinity over the depth is gradual. The salinity equation reads:

31

$$A_s \frac{\partial S}{\partial t} + Q \frac{\partial S}{\partial x} - \frac{\partial}{\partial x} \left( AD \frac{\partial S}{\partial x} \right) = 0 \quad (1)$$

32 Here,  $S$  [psu] is the salinity of the water,  $Q$  [ $L^3 T^{-1}$ ] is the water flow in the estuary,  $A$  [ $L^2$ ] is the  
33 cross-sectional area of the flow (not necessarily equal to the storage cross-section  $A_s$ ), and  $D$  [ $L^2 T^{-1}$ ]  
34 is the dispersion coefficient. The first term reflects the change of the salinity over time as a result of  
35 the balance between the advection by the water flow (second term) and the mixing of water with  
36 different salinity by dispersive exchange flows (third term). If there is no other source of salinity,  
37 then the sum of these terms is zero. If we average this equation over a tidal period, then the first  
38 term reflects the long term change of the salinity as a result of the balance between the advection of  
39 fresh water from the river, and the tidal average exchange flows. In a steady state, where the first  
40 term is zero, the equation can be simply integrated with respect to  $x$ , yielding:  
41

42

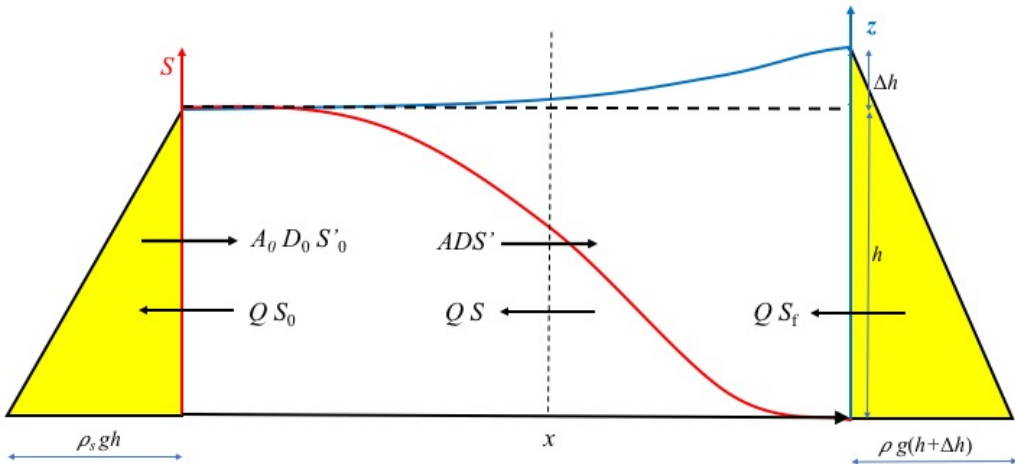
$$Q(S - S_f) - AD \frac{\partial S}{\partial x} = 0 \quad (2)$$

43 with the condition that at the upstream boundary  $\partial S / \partial x = 0$  and  $S = S_f$ , the salinity of the fresh river  
44 water. In the steady state situation the discharge  $Q$  then equals the fresh water discharge coming  
45 from upstream, which has a negative value moving seaward; similarly the salinity gradient is  
46 negative with the salinity decreasing in upstream direction. Assuming that in a given estuary the  
47



48 geometry  $A(x)$  is known, as well as the observed salinity and discharge of the fresh river water, then  
 49 this differential equation has two unknowns  $D(x)$  and  $S(x)$ .

50  
 51 In the steady state salt balance equation the flushing out of salt by the fresh river discharge is  
 52 balanced by the exchange of saline and fresh water resulting from a combination of mixing  
 53 processes that cause an upriver flux of salt. The sketch in Figure 1 presents the system description  
 54 with a typical longitudinal salinity distribution (in red). It also shows the associated water level (in  
 55 blue), which has an upstream gradient due to the decreasing salinity. Because of the density  
 56 difference, the hydrostatic pressures on both sides (in yellow) are not equal. The water level at the  
 57 toe of the salt intrusion curve is  $\Delta h$  higher, resulting in a seaward pressure difference near the  
 58 surface and an inland pressure difference near the bottom. Although the hydrostatic forces (the  
 59 integrals of the hydrostatic pressure distributions) are equal and opposed in steady state, they have  
 60 different working lines, a distance  $\Delta h/3$  apart. This triggers an angular momentum, which drives the  
 61 gravitational circulation.  
 62



63  
 64 **Figure 1.** System description of the salt and fresh water mixing in an estuary, with the seaside on the left and the river side on  
 65 the right. The water level (blue line) has a slope as a result of the salinity distribution (red line). In yellow are the hydrostatic  
 66 pressure distributions on both sides. The black arrows show the boundary fluxes.

67  
 68 The dispersion coefficient is generally determined by calibration on observations, or predicted by  
 69 (semi-)empirical methods. Providing a theoretical basis for the dispersion coefficient is not trivial.  
 70 A fundamental question is what this dispersion actually is. Is it a physical parameter, or merely a  
 71 parameter that follows from averaging the complex turbulent flow patterns in a natural watercourse.  
 72 MacCready (2004), for instance, was able to derive an analytical expression for the dispersion as a  
 73 function of the salinity gradient and geometric, hydraulic and turbulence parameters. But also this  
 74 derivation required simplifying assumptions.  
 75

76 The complication is that there are many different mixing processes at work. One can distinguish:  
 77 tidal shear, tidal pumping, tidal trapping, gravitation circulation (e.g. Fischer et al., 1979) and  
 78 residual circulation due to the interaction between ebb and flood channels (Nguyen and Savenije,



79 2008; Zhang and Savenije, 2017). And these different processes can be split up in many  
80 subcomponents. Park and James (1990), for instance, distinguished 66 components, grouped into 11  
81 terms. This reductionist approach, unfortunately, did not lead to more insight.

82 **2. Applying thermodynamics to salt and fresh water mixing**

83 Here we take a system's approach, where the assumption is that the different mechanisms are not  
84 independent but are jointly at work to reduce the salinity gradient that drives the exchange flows.  
85 We use the concept of Maximum Power, as described by Kleidon (2016). Kleidon defines Earth  
86 system processes as dissipative systems that do conserve mass and energy, but export entropy.  
87 These systems tend to function at maximum power, whereby the power of the system can be  
88 defined as the product of a process flux and the gradient driving the flux. The ability to maintain  
89 this power (i.e., work through time) in steady state results from the exchange fluxes at the system  
90 boundary, and when work is performed at the maximum possible rate within the system  
91 ("Maximum Power"), this state reflects the conditions at the system boundary. The key parameter  
92 describing the process can then be found by maximizing the power.

93 From an energy perspective, we see that the fresh water flux, which has a lower density than saline  
94 water and, without a counteracting process, would float on top of the saline water, adds potential  
95 energy to the system, while the tide, which flows in and out of the estuary at a regular pace, creates  
96 turbulence, mixes the fresh and saline water and hence works at reducing this potential energy. This  
97 is why dispersion predictors are generally linked to the Estuarine Richardson number, which  
98 represents the ratio of the potential energy of the fresh water entering the estuary to the kinetic  
99 energy of the tidal flow.

100 In thermodynamic terms, the fresh water flux maintains a potential energy gradient, which triggers  
101 mixing processes that work at depleting this gradient. Because the strength of the mixing of fresh  
102 and saline water in turn depends on this gradient, there is an optimum where the mixing process  
103 performs at maximum power. From a system point of view, it is not really relevant which particular  
104 mixing process is dominant, or how these different processes jointly reduce the salinity gradient.  
105 What is relevant is how the optimum flux associated with this mixing process, yielding maximum  
106 power, depends on the dispersion.

107 In our case, the power derived from the potential energy of the fresh water flux is described by the  
108 product of the upstream dispersive water flux and the gradient in geopotential height driving this  
109 flux, or alternatively, the product of the dispersive exchange flux and the water level gradient.

110 The water level gradient follows from the balance between the hydrostatic pressures of fresh and  
111 saline water (see e.g. Savenije, 2005), resulting in:

$$112 \frac{\partial z}{\partial x} = -\frac{h}{2\rho} \frac{\partial \rho}{\partial x} \quad (3)$$

113 where  $z$  [L] is the tidal average water level,  $h$  [L] is the tidal average water depth and  $\rho$  [ML<sup>-3</sup>] is the  
114 density of the saline water. Note that this equation applies to the case where the river flow velocity  
115 is small, which is the case when estuaries are well mixed. Otherwise a backwater effect should be  
116 included, but this only applies to a situation of high river discharge when the salt intrudes by means  
117 of a salt wedge with a sharp interface.

118 One can express the density of saline water as a function of the salinity  $S$  [psu]:  $\rho = 1000 + \alpha_1 S$   
119 ( $\text{kg/m}^3$ ) where  $\alpha_1$  is a constant with a value of about 25/35, because seawater with a salinity of 35  
120 psu has a density of about  $1025 \text{ kg/m}^3$ . As a result, eq.(3) can be written as:



127 
$$\frac{\partial z}{\partial x} = -\alpha_1 \frac{h}{2\rho} S' \quad (4)$$

128 The upstream dispersive flux is implicit in the salt balance equation, which in steady state can be  
 129 written as:

130

131 
$$Q(S - S_f) = ADS' \quad (5)$$

132 where  $S' [L^{-1}]$  is the salinity gradient, which is negative in upstream direction. So the left hand term  
 133 is the salt flux due to the fresh water of the river that pushes back the salt, whereas the right hand  
 134 term is the dispersive intrusion of salt due to the exchange flux of the combined mixing processes  
 135 (see Figure 1). Writing both sides as water fluxes results in:

136 
$$Q = \frac{ADS'}{(S - S_f)} \quad (6)$$

137 The right hand side is the water exchange flux, which is the flux that depletes the gradient. As (6)  
 138 shows, in steady state this exchange flux is equal to the fresh water discharge. Combination of the  
 139 flux and the gradient leads to the power of the mixing system per unit length (defined as a positive  
 140 quantity):

141 
$$P = -\rho g Q \frac{\partial z}{\partial x} = \alpha_1 Q \frac{gh}{2} S' \quad (7)$$

142 To apply the theory of maximum power to the dispersive process, we need to maximize the power  
 143 with regard to the dispersion coefficient, which is the parameter representing the mixing and which  
 144 is the main unknown in salt intrusion prediction:

145 
$$\frac{\partial P}{\partial D} = 0 \quad (8)$$

146 Applying (8) with constant river discharge  $Q$  and constant depth  $h$  -- the property of an ideal  
 147 alluvial estuary, according to Savenije (2005) -- leads to:

148 
$$\frac{\partial S'}{\partial D} = 0 \quad (9)$$

149 Using the salt balance equation, where  $S' = Q(S - S_f)/(AD)$ , differentiation leads to:

150 
$$\frac{S'}{(S - S_f)} \left\{ \frac{S'}{D'} - \frac{A'(S - S_f)}{AD'} - \frac{(S - S_f)}{D} \right\} = 0 \quad (10)$$

151

152 The solution  $S' = 0$  is trivial. For non-zero salinity gradient, the solution is:

153 
$$\frac{DS'}{(S - S_f)D'} = \frac{A'D}{AD'} + 1 \quad (11)$$

154

155 We introduce three length scales:  $a = -(A - A_f)/A'$ ,  $s = -(S - S_f)/S'$  and  $d = -D/D'$ , where  $a$  is  
 156 the convergence length of an exponentially varying estuary cross-section which tends towards the  
 157 cross-section of the river  $A_f$ ,  $s$  is length scale of the longitudinal salinity variation, and  $d$  is length  
 158 scale of the longitudinal variation of dispersion. In macro-tidal estuaries, the part of the estuary  
 159 where the salt intrusion occurs has a much larger cross-section than the upstream river, such that  
 160  $A_f \ll A$  and  $a \approx A/A'$ . In riverine estuaries, where this is not the case, a factor  $\varepsilon = (1 - A_f/A)$  should be  
 161 included. All length scales have the dimension of [L]. In an exponentially shaped estuary, the  
 162 convergence length is a constant, but  $d$  and  $s$  vary with  $x$ . It can be shown that the proportion  $s/d$   
 163 equals the Van der Burgh coefficient  $K = AD'/Q$ , which in this approach varies as a function of  $x$ ,



164 although generally assumed constant (e.g. Savenije, 2005; and Zhang and Savenije, 2017). Using  
165 these length scales, eq. (11) can be written as:

166 
$$\frac{s}{d} = \frac{a}{a+d\varepsilon} \quad (12)$$

167 or:

168 
$$s = \frac{ad}{a+d\varepsilon} \quad (12a)$$

169 or:

170 
$$d = \frac{as}{a-s\varepsilon} \quad (12b)$$

172 where in estuaries with a pronounced funnel shape  $\varepsilon \approx 1$ . Eq.(12) is an additional equation to the salt  
173 balance, which in terms of the length scales reads:  $s = -AD/Q$ . As a result, we have two  
174 differential equations with two unknowns:  $S(x)$  and  $D(x)$ . Adding two boundary conditions at a  
175 given point  $x=0$ :  $S_0$  and  $D_0$  would solve the system. The first boundary condition is simply sea  
176 salinity if the boundary is chosen at the estuary mouth. Then the only unknown parameter left is the  
177 value for the dispersion at the ocean boundary. For this boundary value empirical predictive  
178 equations have been developed which relate the  $D_0$  to the Estuarine Richardson number (e.g. by  
179 Gisen et al., 2015), which goes beyond this paper. If observations of salinity distributions are  
180 available, then the value of  $D_0$  is obtained by calibration.

181  
182 What the maximum power equation has contributed is that it provides an additional equation. In the  
183 past, a solution could only be found if an empirical equation was added describing  $D(x)$ , containing  
184 an additional calibration parameter. In the approach by Savenije (2005) this was the empirical Van  
185 der Burgh equation containing the constant Van der Burgh coefficient  $K$ . However, with the new  
186 equation (12), which in fact represents a spatially varying Van der Burgh coefficient, this additional  
187 calibration parameter is no longer required. So this new approach replaces and empirical equation  
188 for a physically based equation and reduces the number of calibration parameters to one: the  
189 dispersion at a well-chosen boundary condition.

190

### 191 **3. Application**

192 The two equations (2) and (12) together can be solved numerically by a simple linear integration  
193 scheme. As boundary condition it requires values for  $S(x_1)$  and  $D(x_1)$  at a well-chosen location  $x=x_1$ .  
194 In alluvial estuaries the cross-sectional area  $A(x)$  generally varies according to an exponential  
195 function which often has an inflection point (see for example Figure 2 describing the Maputo  
196 Estuary in Mozambique). The boundary condition is best taken at this inflection point if the estuary  
197 has one. If the estuary has no inflection point, as is the case in the Limpopo estuary (see Figure 3),  
198 then the boundary condition is taken at the estuary mouth.

199

200 The downstream part of estuaries with an inflection point has a much shorter convergence length,  
201 giving the estuary a typical trumped shape. This wider part is generally not longer than about 10  
202 km, which is the distance over which ocean waves dissipate their energy. Beyond the inflection  
203 point, the shape is determined by the combination of kinetic energy of the tide and the potential  
204 energy of the river flow. If the tidal energy is dominant over the potential energy of the river, then  
205 the convergence is short, leading to a pronounced funnel shape; if the potential energy of the river is  
206 large due to regular and substantial flood flows, then the convergence is large, typical for deltas.  
207 Hence, the topography can be described by two branches:



209 
$$A = A_f + (A_0 - A_f) \exp(-x/a_0) \text{ if } 0 < x < x_1 \quad (13)$$

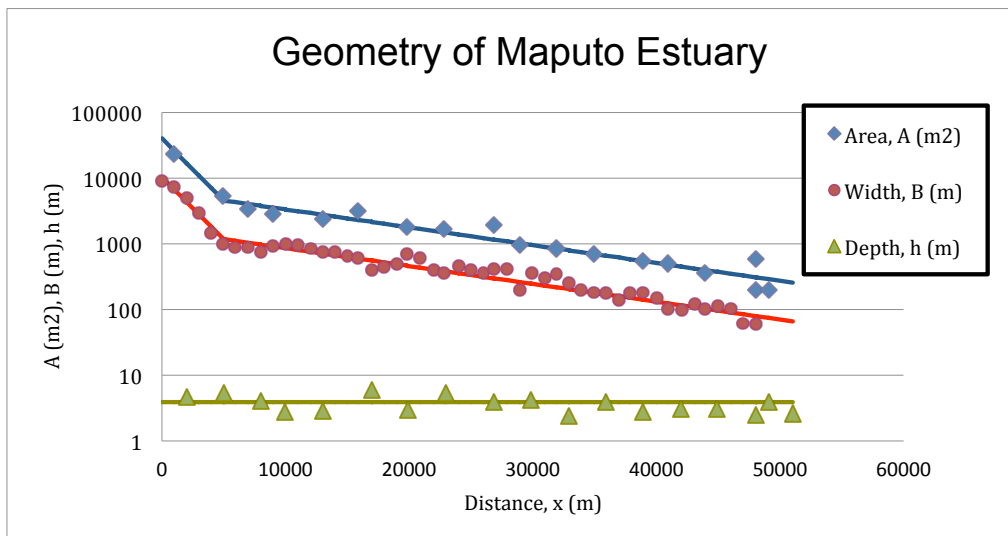
210 
$$A = A_f + (A_1 - A_f) \exp(-(x - x_1)/a_1) \text{ if } x \geq x_1$$

211 where  $A_0$  and  $A_1$  are the cross-sectional areas at  $x=0$  and  $x=x_1$ , respectively, and  $a_0$  and  $a_1$  are the  
212 convergence lengths of the lower and upper segments. In some cases, where ocean waves don't  
213 penetrate the estuary, there is no inflection point and  $x_1=0$ . The Maputo (see Figure 2) has two  
214 segments, whereas the Limpopo Estuary (see Figure 3), an estuary in Mozambique 200 km north of  
215 the Maputo semi-closed by a sand bar, has a single branch. It can also be seen that in the Limpopo  
216 the size of the river cross-section is not negligible and that  $\varepsilon < 1$  showing a slight curve in the  
217 exponential functions.

218 Subsequently we have integrated the equations (2) and (12) conjunctively by a simple explicit  
219 numerical scheme in a spreadsheet and confronted the solution with observations. The solutions are  
220 fitted to the data by selecting values for  $S$  and  $D$  at the boundary condition  $x=x_1$  (or at  $x=0$  for the  
221 Limpopo). Figures 4 and 5 show applications of the solution to selected observations in the Maputo  
222 and Limpopo estuaries. In the supplementary material more applications are shown, also for other  
223 estuaries in different parts of the world.

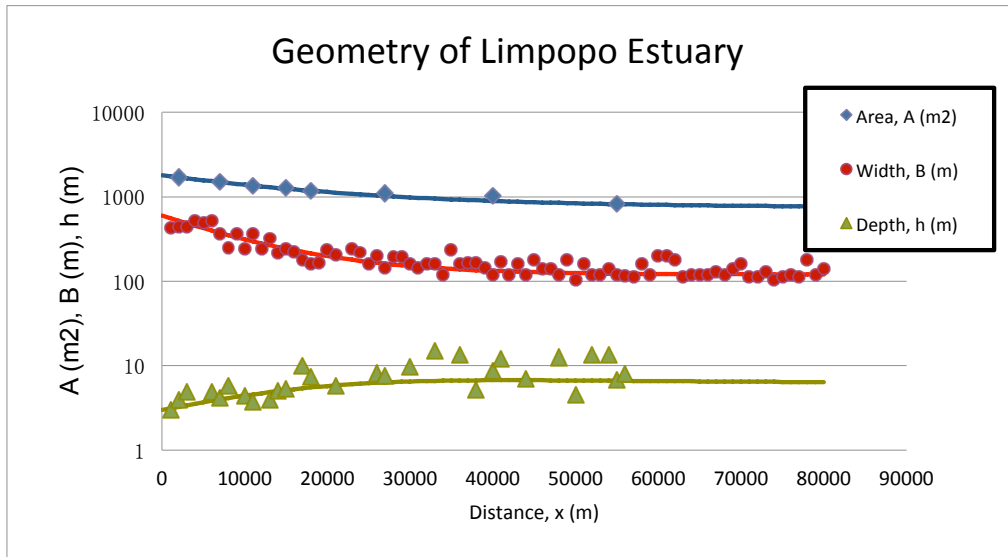
224  
225

226



227  
 228  
 229  
 230

Figure 2. Geometry of the Maputo Estuary, showing the cross-sectional area  $A$  (blue diamonds), the width  $B$  (red dots) and the depth  $h$  (green triangles) on a logarithmic scale, as a function of the distance from the mouth. The inflection point at  $x_1=5000 \text{ m}$  separates the lower segment with a convergence length of  $a_0=2300 \text{ m}$  from the upper segment with  $a_1=16000 \text{ m}$ .

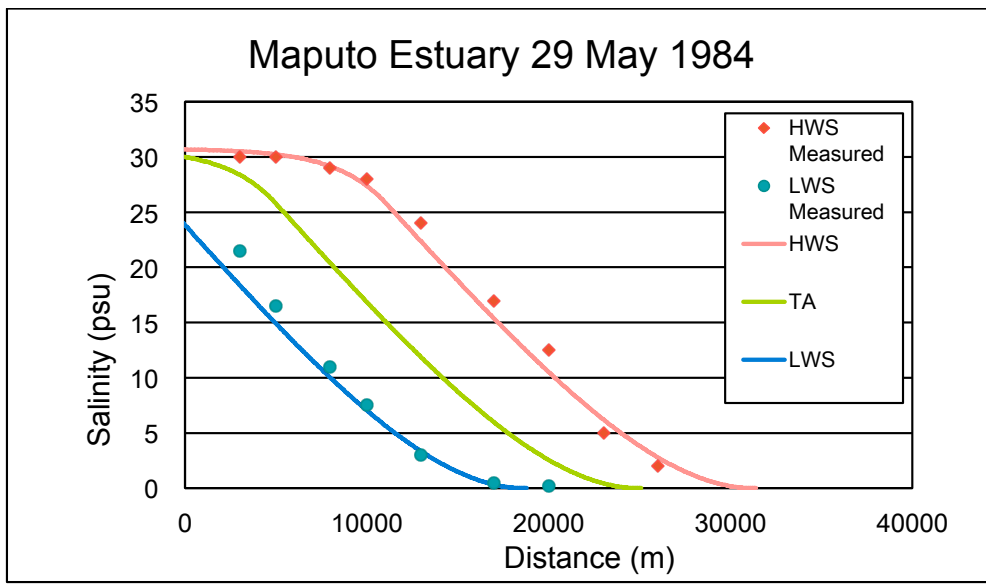


231  
 232  
 233  
 234

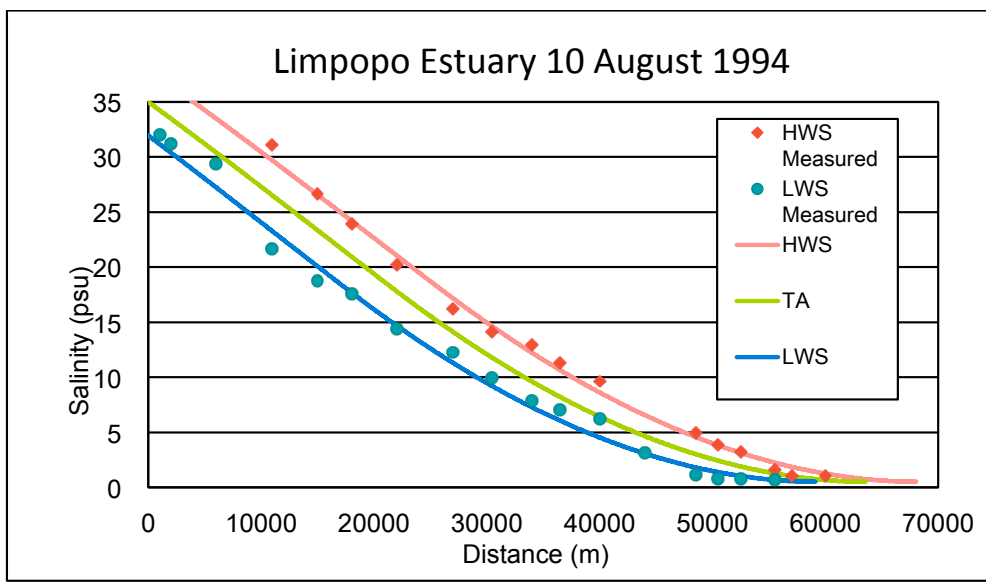
Figure 3. Geometry of the Limpopo Estuary, showing the cross-sectional area  $A$  (blue diamonds), the width  $B$  (red dots) and the depth  $h$  (green triangles) on a logarithmic scale, as a function of the distance from the mouth. There is no inflection point, but the estuary converges exponentially towards the river cross-section  $A_f=800 \text{ m}^2$ , with a convergence length of 20 km.



235



236  
237 Figure 4. Application of the numerical solution to observations in the Maputo Estuary for high water slack (HWS)  
238 and low water slack (LWS). The green line shows the tidal average (TA) condition. The red diamonds reflect the observations at HWS  
239 and the blue dots the observations at LWS on 29 May 1984.



240  
241 Figure 5. Application of the numerical solution to observations in the Limpopo Estuary for high water slack (HWS)  
242 and low water slack (LWS). The green line shows the tidal average (TA) condition. The red diamonds reflect the observations at HWS  
243 and the blue dots the observations at LWS on 10 August 1994.

244  
245



246 **4. Discussion and conclusion**

247 Making use of the Maximum Power (MP) concept, it was possible to derive an additional equation  
248 to describe the mixing of salt and fresh water in estuaries. Together with the salt balance equation  
249 these two first order and linear differential equations only require two boundary conditions (the  
250 salinity and the dispersion at some well-chosen boundary) to be solved. If the estuary has an  
251 inflection point in the geometry, then the preferred boundary condition lies there, otherwise the  
252 boundary condition is chosen at the ocean boundary.

253 This new equation can replace previous empirical equations, such as the Van der Burgh  
254 equation, and does not require any calibration coefficients (besides the boundary conditions). The  
255 new equation appears to fit very well to observations, which adds credibility to the correctness of  
256 applying the MP concept to fresh and salt water mixing.

257 The method presented here is based on a system's perspective, which is holistic rather than  
258 reductionist. Reductionist theoretical methods have tried to break down the total dispersion in a  
259 myriad of smaller mixing processes, some of which are difficult to identify or to connect to  
260 conditions that make them more or less prominent. The idea here is that in a freely adjustable  
261 system, such as an alluvial estuary, individual mixing processes are not independent of each other,  
262 but rather influence each other and jointly work at reducing the salinity gradient at maximum  
263 dissipation. The resulting level of maximum power and dissipation is set by the boundary  
264 conditions of the system. It then is less important which mechanism is dominant, as long as the  
265 combined performance is correct. The maximum power limit is a way to derive this joint  
266 performance of mixing processes. The fact that the relationship derived from maximum power  
267 works so well in a wide range of estuaries, is an indication that natural systems evolve towards  
268 maximum power, much like a machine that approaches the maximum performance of the Carnot  
269 limit.

270

271 **References:**

272

273 Fischer, H. B., List, E. J., Koh, R. C. Y., Imberger, J. and Brooks, N. H. (1979) Mixing in Inland  
274 and Coastal Waters, Academic Press.

275

276 Gisen, J. I. A., Savenije, H. H. G., and Nijzink, R. C.: Revised predictive equations for salt intrusion  
277 modelling in estuaries, *Hydrol. Earth Syst. Sci.*, 19, 2791-2803, doi:10.5194/hess-19-2791-2015,  
278 2015.

279

280 Kleidon, A. (2016). Thermodynamic foundations of the Earth system. Cambridge University Press.

281

282 MacCready, P. (2004). Toward a unified theory of tidally-averaged estuarine salinity structure.  
283 *Estuaries*, 27(4), 561-570.

284

285 Nguyen, A. D., Savenije, H. H. G., van der Wegen, M., & Roelvink, D. (2008). New analytical  
286 equation for dispersion in estuaries with a distinct ebb-flood channel system. *Estuarine, coastal and*  
287 *shelf science*, 79(1), 7-16.

288

289 Park, J. K., & James, A. (1990). Mass flux estimation and mass transport mechanism in estuaries.  
290 *Limnology and Oceanography*, 35(6), 1301-1313.

291

292 Savenije, H. H. G. (2005). Salinity and tides in alluvial estuaries. Elsevier.

293



294 Zhang Z. & Savenije, H.H.G., The physics behind Van der Burgh's empirical equation, providing a  
295 new predictive equation for salinity intrusion in estuaries, (2017). *Hydrol. Earth Syst. Sci.*, 21,  
296 3287–3305, <https://doi.org/10.5194/hess-21-3287-2017>  
297  
298  
299  
300  
301  
302